Chinese Physics Letters

LETTER

Canonical Quantum Mpemba Effect in a Dissipative Qubit

Cite as: Xingli Li *et al*. 2026 *Chin. Phys. Lett.* **43** 090603

DOI CSTR

Recommended Articles

Signatures of Environment-Induced Quantum Synchronization Transitions via Two-body Dissipator Engineering
Xingli Li, Yan Li, and Yangqian Yan
Chin. Phys. Lett. **43**, 020302 (2026)

An Off-Resonant Quantum Collision Model: Realizing a Qubit Coupled with an Effective Negative-Temperature Bath
Wei-Bin Yan, Zhong-Xiao Man, Ying-Jie Zhang, and Yun-Jie Xia
Chin. Phys. Lett. **42**, 010203 (2025)

High-Fidelity Two-Qubit Quantum Logic Gates in a Trapped-Ion Chain Using Axial Motional Modes
Xingyu Zhao, Ji Bian, Yi Li, Yue Li, Mengxiang Zhang, and Yiheng Lin
Chin. Phys. Lett. **42**, 110601 (2025)

Symmetry Breaking Dynamics in Quantum Many-Body Systems
Hui Yu, Zi-Xiang Li, and Shi-Xin Zhang
Chin. Phys. Lett. **42**, 110602 (2025)

Variational Quantum Algorithms for the Steady States of Open Quantum Systems
Huan-Yu Liu, Tai-Ping Sun, Yu-Chun Wu, and Guo-Ping Guo
Chin. Phys. Lett. **38**, 080301 (2021)

A series journal of Chinese Physical Society distributed by IOP Publishing

Chinese Physics Letters

Chin. Phys. Lett. **43** 090603 (2026)

LETTER

DOI: 10.1088/0256-307X/43/9/090603
CSTR: 32039.14.0256-307X.43.9.090603

Canonical Quantum Mpemba Effect in a Dissipative Qubit

Xingli Li[1], Yan Li[1], and Yangqian Yan[1,2,3,*]

[1]Department of Physics, The Chinese University of Hong Kong, Hong Kong, China
[2]State Key Laboratory of Quantum Information Technologies and Materials, The Chinese University of Hong Kong, Hong Kong, China
[3]The Chinese University of Hong Kong Shenzhen Research Institute, Shenzhen 518057, China

[*]Corresponding author. Email: yqyan@cuhk.edu.hk

The Mpemba effect, where a hotter system cools faster than a colder one under otherwise identical conditions, has been extensively studied in classical systems. In this work, we present the quantum analogue of the Mpemba effect using a dissipative qubit, which is referred to as the canonical quantum Mpemba effect. We demonstrate that, under identical conditions, the relaxation dynamics of a qubit initialized in a thermal state with a higher temperature can be exponentially faster than that of a colder thermal state. Strikingly, for a fixed Liouvillian, this acceleration can be selected solely by varying the initial temperature, rather than by applying a specially designed unitary transformation to the initial state. The existence and value of the critical temperature nevertheless depend on the system and dissipation parameters. The relaxation is characterized as an overall cooling process: the system evolves from a higher-temperature, higher-energy thermal state toward a steady state with a lower effective temperature and energy, mirroring its classical counterpart. Last, we propose a practical classical–quantum hybrid algorithmic quantum circuit to simulate the dissipative evolution of thermal states and validate its experimental feasibility using superconducting qubits.

Introduction

Anomalous relaxation dynamics in non-equilibrium systems have attracted significant attention, with the Mpemba effect [1] being a well-known example. This phenomenon, where a system prepared at a higher initial temperature can relax faster than one at a lower temperature, has been extensively analyzed in classical systems, revealing its dependence on initial states and system properties. Recently, this counterintuitive phenomenon has been extended to the quantum realm [2–9], where studies have investigated anomalous relaxation dynamics in both closed [10–23] and open quantum systems [24–50]. Furthermore, experimental demonstrations on quantum simulation platforms [51–54] have confirmed its feasibility, highlighting the universality of the Mpemba effect in quantum systems.

The manifestation of the Mpemba effect differs between closed and open quantum systems. In closed quantum systems, it refers to the anomalous phenomenon where a more asymmetric initial state restores the system's symmetry faster than a less asymmetric one [10–16]. By contrast, in open quantum systems, the Mpemba effect is defined as an exponentially accelerated relaxation to the steady state [24–33]. This acceleration is achieved through the careful engineering of initial states via unitary transformations, and this state engineering exploits a key mechanism in open quantum systems: suppression of contributions from the Liouvillian's slowest-decaying eigenmode [24].

To set the stage, the top panel of Fig. 1(a) illustrates the conventional quantum Mpemba effect in open quantum systems: the crossing of the trace-distance curves indicates that one initial state relaxes faster to the steady state. This distance-based criterion does not specify whether either trajectory is cooling or heating and therefore does not ensure the thermodynamic directionality of the classical Mpemba effect, which involves cooling processes. In addition, in open quantum systems the steady-state temperature $T_{\rm SS}$ need not coincide with any bath temperature, especially in the presence of multiple baths, coherence, or other non-equilibrium features; an effective steady-state temperature must therefore be defined. These observations motivate a stronger, thermodynamically consistent formulation that we call the canonical quantum Mpemba effect, characterized by two requirements: (i) Thermodynamic directionality—both relaxation trajectories are overall cooling processes, with $T_{\rm high} > T_{\rm low} > T_{\rm SS}$; and (ii) Exponential acceleration—the hotter initial thermal state exhibits exponential speedup via suppression of the slowest Liouvillian mode. The lower panel of Fig. 1(a) illustrates this canonical regime.

In this Letter, we use a simple yet fundamental open quantum system to demonstrate the canonical quantum Mpemba effect: a qubit coupled to two independent thermal baths, with each bath engineering a distinct dissipation channel [Fig. 1(b)]. Our key findings are as follows: (1) By defining the steady-state effective temperature $T_{\rm SS}$ as the temperature of the thermal state that minimizes the trace distance to the steady state, we identify relaxation dynamics that fulfill the criteria for the canonical quantum Mpemba effect, wherein a higher initial temperature suppresses the slowest relaxation mode, thus enabling an exponentially accelerated overall cooling process. Unlike protocols that suppress the slowest Liouvillian mode through a specially designed unitary transformation of the initial state, our approach achieves the same suppression solely by varying the temperature of the initial Gibbs state for a fixed Liouvillian. (2) We propose a quantum collision-model scheme to simulate the dissipative evolution of thermal states with current quantum technologies. The feasibility of the classical–quantum hybrid implementation [Fig. 1(c)] is validated using superconducting-qubit circuits.

Model

We consider a qubit system with Hamiltonian $H_{\rm S} = \omega_y\sigma_{\rm S}^y + \omega_z\sigma_{\rm S}^z$, where $\sigma_{\rm S}^{y(z)}$ are the Pauli operators and $\omega_{y(z)}$ are the frequencies ($\hbar = k_{\rm B} = 1$ hereinafter). The initial states are thermal states: $\varrho_{\rm th}[T] = \exp(-\beta H_{\rm S})/\mathcal{Z}$, where $\mathcal{Z} = {\rm Tr}[\exp(-\beta H_{\rm S})]$ is the partition function and $\beta = 1/k_{\rm B}T$ is the inverse temperature. The dynamics of this system are governed by the Lindblad master equation [55]

$$\frac{\rm d}{{\rm d}t}\varrho = -{\rm i}[H_{\rm S}, \varrho] + \gamma_-\mathcal{D}_\varrho[\sigma_-] + \gamma_y\mathcal{D}_\varrho[\sigma_y], \tag{1}$$

where $\mathcal{D}_\varrho[o] = o\varrho o^\dagger - (o^\dagger o\varrho + \varrho o^\dagger o)/2$ denotes the dissipator, and σ_- and σ_y are the jump operators with respective rates γ_- and γ_y. We set $\gamma_- = \gamma_y = \gamma$ for simplicity. The Lindblad master equation describes

Received 27 March 2026; accepted 24 August 2026; published 17 September 2026

© 2026 Chinese Physical Society and IOP Publishing Ltd. All rights, including for text and data mining, AI training, and similar technologies, are reserved.

Check for updates

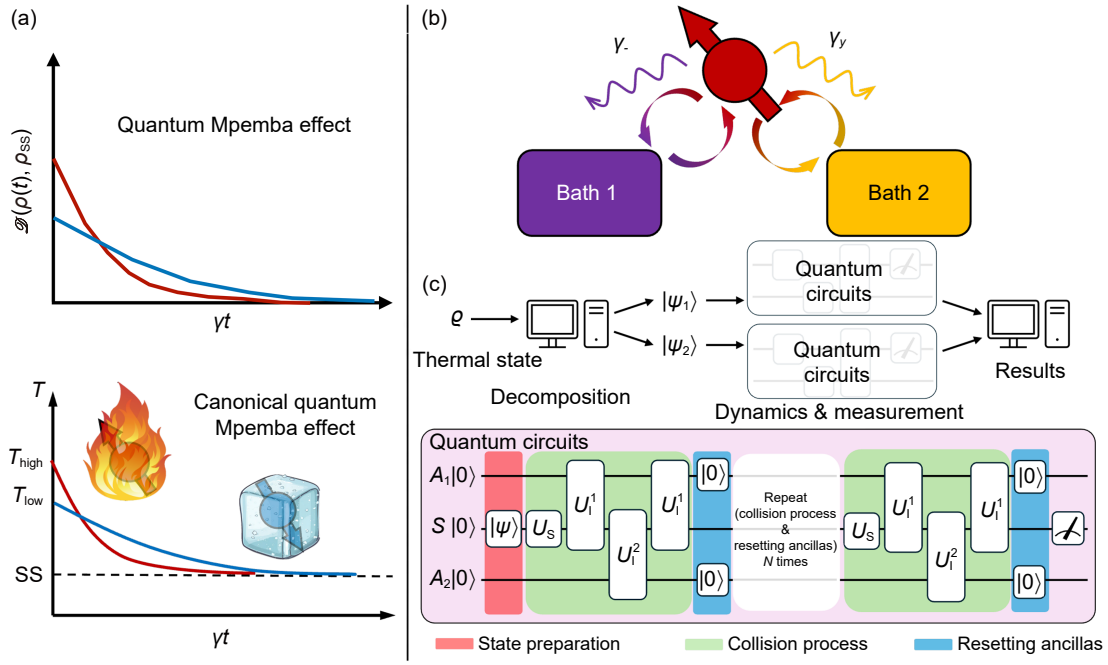

Fig. 1. (a) Schematic comparison between the conventional and canonical quantum Mpemba effects in open quantum systems. Top panel: the conventional effect is identified by a crossing of the trace-distance curves, indicating faster relaxation to the steady state. Bottom panel: the canonical quantum Mpemba effect considered in this paper additionally requires both relaxations to be overall cooling processes. (b) Schematic of the model: a qubit coupled to two independent baths, each inducing a distinct dissipation channel with decay rates γ_- and γ_y. (c) Schematic of the collision-model circuit used in the classical–quantum hybrid simulation of dissipative evolution from a thermal initial state.

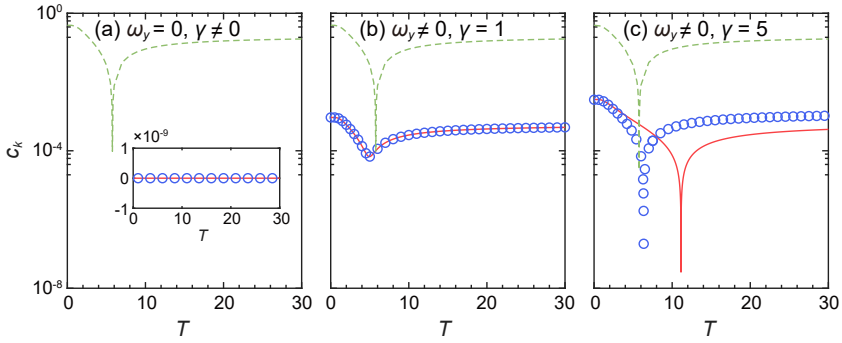

Fig. 2. The overlaps c_k between the eigenmodes l_k and the initial thermal state as a function of its temperature T. The overlaps c_2 (red solid), c_3 (blue circles), and c_4 (green dashed) are plotted, with $\omega_z = 2$ fixed throughout. (a) In the absence of the off-diagonal term ω_y, the inset shows that c_2 and c_3 are always zero. (b) For finite off-diagonal term $\omega_y = 0.01$ and weak dissipation $\gamma = 1$, c_2, and c_3 overlap and are smooth. (c) For finite off-diagonal term $\omega_y = 0.01$ and strong dissipation $\gamma = 5$, the sharp dip of c_2 at $T = 11.13$ indicates the potential for the canonical quantum Mpemba effect.

open quantum system dynamics via the Liouvillian $\mathcal{L}$ [24], defined by the linear map $\mathrm{d}\varrho/\mathrm{d}t = \mathcal{L}[\varrho]$. The Liouvillian can be represented in matrix form and, away from a Liouvillian exceptional point (LEP), is diagonalizable, with right eigenoperators satisfying $\mathcal{L} r_k = \lambda_k r_k$ and left eigenoperators satisfying $\mathcal{L}^\dagger l_k = \lambda_k^* l_k$, where the eigenvalues λ_k are complex numbers with $\mathrm{Re}(\lambda_k) \leq 0, \forall k$ [55]. We order λ_k by descending real part: $\mathrm{Re}(\lambda_{d^2}) \leq \cdots \leq \mathrm{Re}(\lambda_2) \leq \mathrm{Re}(\lambda_1) = 0$, with d being the dimension of the Hilbert space. Therefore, away from an exceptional point, the evolution of a given initial state ϱ_{ini} takes the form

$$\varrho(t) = \exp(t\mathcal{L})[\varrho_{\mathrm{ini}}] = \varrho_{\mathrm{SS}} + \sum_{k=2}^{d^2} \mathrm{Tr}[l_k \varrho_{\mathrm{ini}}] r_k \exp(\lambda_k t), \tag{2}$$

where $\varrho_{\mathrm{SS}} = r_1/\mathrm{Tr}[r_1]$ denotes the steady state, and $c_k = |\mathrm{Tr}[l_k \varrho_{\mathrm{ini}}]|$ denotes the overlap between the initial state ϱ_{ini} and left eigenoperators l_k. In the long-time limit ($t \to \infty$), the relaxation is dominated by the slowest eigenmode; thus, the timescale for relaxation is $\tau = |\mathrm{Re}(\lambda_2)|^{-1}$. Equation (2) implies that suppressing the slowest mode accelerates the relaxation process, which requires its overlap c_2 to approach zero. This means the temperature dependence of the overlaps c_k indicates whether relaxation is accelerated. To this end, we discuss the behaviors of c_k versus the initial thermal state's temperature T.

Figure 2 shows the variation of c_k as a function of T. This encompasses the three scenarios of Eq. (1), defined by the off-diagonal term in the Hamiltonian ω_y (either zero or finite) and the dissipation strength γ (either weak or strong). We find that in the absence of the off-diagonal term ($\omega_y = 0$) [Fig. 2(a)], the behaviors of c_k are independent of the dissipation strength. Moreover, c_2 and c_3 remain zero at all times, which implies that the dynamics are solely governed by the fastest-decaying mode, and the relaxation cannot be accelerated. This behavior can be explained by the diagonal Hamiltonian, which prepares an initial thermal state devoid of coherence. The jump operator σ_- then drives relaxation at the fastest possible rate, leaving no room for acceleration. Introducing a slight off-diagonal term ($\omega_y = 0.01$) dramatically alters the scenarios [Figs. 2(b) and 2(c)]. Under weak dissipation [Fig. 2(b)], although c_2 and c_3 vary with temperature, c_2 never approaches zero, precluding acceleration. In contrast, under strong dissipation, c_2 plummets near $T \approx 11.13$, suggesting a potential canonical Mpemba effect. Confirmation, however, requires verifying that the steady-state effective temperature lies below this potential acceleration temperature.

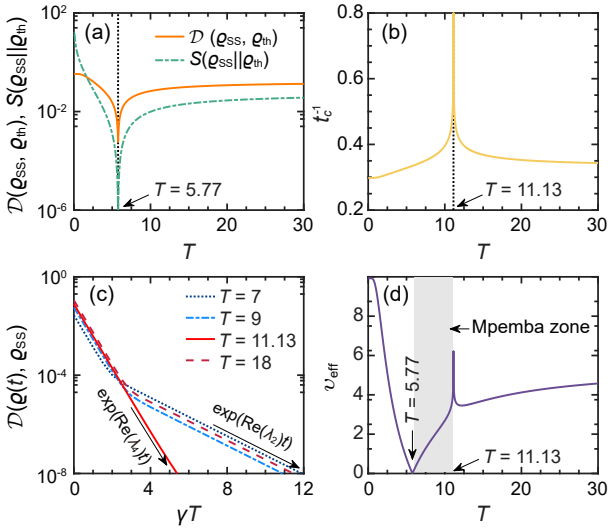

Fig. 3. (a) The trace distance $D(\varrho_{\rm SS}, \varrho_{\rm th}[T])$ (orange solid line) and quantum relative entropy $S(\varrho_{\rm SS}\|\varrho_{\rm th}[T])$ (green solid line) between the steady state and the thermal states as a function of temperature T. The dashed line indicates that when $T \approx 5.77$, the distance between $\varrho_{\rm SS}$ and $\varrho_{\rm th}[T]$ is minimized; i.e., the steady state is best described by a thermal state at $T \approx 5.77$. (b) The inverse critical time $t_{\rm c}^{-1}$ to reach the steady state as a function of the initial-state temperature T. The dashed line indicates that the initial thermal state at $T \approx 11.13$ reaches the steady state the fastest. (c) Trace distance between the time-evolved state $\varrho(t)$ and the steady state $\varrho_{\rm SS}$ as a function of the dimensionless time γt for different initial temperatures. (d) The effective velocity $v_{\rm eff}$, i.e., the ratio of the initial trace distance to the critical time, as a function of the initial-state temperature T. The gray zone with $T \in [5.77, 11.13]$ indicates the region where the canonical quantum Mpemba effect occurs.

The Steady-State Effective Temperature

Since the steady state of an open system cannot always be characterized by the Gibbs ensemble, $\varrho_{\rm SS} \not\propto \exp(-\beta H_{\rm S})$ [56,57], we determine $T_{\rm SS}$ by the thermal state with the shortest distance to the steady state,

$$T_{\rm SS} = \arg\min_{T>0}\{D(\varrho_{\rm SS}, \varrho_{\rm th}[T])\}, \tag{3}$$

where $D(\varrho_{\rm a}, \varrho_{\rm b})$ is the trace distance [58] defined as

$$D(\varrho_{\rm a}, \varrho_{\rm b}) = \frac{1}{2}{\rm Tr}\left[\sqrt{(\varrho_{\rm a}-\varrho_{\rm b})^{\dagger}(\varrho_{\rm a}-\varrho_{\rm b})}\right]. \tag{4}$$

Trace distance is a metric that quantifies the distinguishability between two states, ranging from 0 (indistinguishable) to 1 (perfectly distinguishable). Furthermore, we consider quantum relative entropy [58] as an alternative measure of the difference between two states, defined as

$$S(\varrho_{\rm a}\|\varrho_{\rm b}) = {\rm Tr}[\varrho_{\rm a}\log\varrho_{\rm a} - \varrho_{\rm a}\log\varrho_{\rm b}]. \tag{5}$$

Quantum relative entropy reflects the informational difference between two states. It is asymmetric and quantifies how much one state deviates from another.

Figure 3(a) shows the trace distance $D(\varrho_{\rm SS}, \varrho_{\rm th}[T])$ and the quantum relative entropy $S(\varrho_{\rm SS}\|\varrho_{\rm th}[T])$ for $T > 0$. The trace distance reaches $D_{\rm min} = 5.7867 \times 10^{-4}$ at $T_{\rm SS} \approx 5.77$; hence, the steady state is close to, but not exactly, a Gibbs state of $H_{\rm S}$. The relative entropy reaches its minimum, $S_{\rm min} = 6.9632 \times 10^{-7}$, at the same temperature. This agreement confirms that the extracted $T_{\rm SS}$ is consistent for the two measures.

Quantum Mpemba Effect

After determining the steady-state effective temperature, we now check whether the canonical quantum Mpemba effect occurs. In Fig. 3(b), we show the inverse critical time $t_{\rm c}^{-1}$ as a function of temperature. The critical time $t_{\rm c}$ is defined as the time when the trace distance between the time-evolved state $\varrho(t)$ and $\varrho_{\rm SS}$ reaches a threshold value, which we set as $D(\varrho(t), \varrho_{\rm SS}) \sim 10^{-8}$. The yellow solid line in Fig. 3(b) shows that the inverse critical time $t_{\rm c}^{-1}$ begins at approximately 0.298 at zero temperature and increases with rising temperature. When the temperature approaches $T \approx 11.13$, the inverse critical time reaches a maximum value. This indicates that the system is accelerated to reach the steady state at this temperature, as predicted by the overlap c_2 in Fig. 2(c).

To better demonstrate the relaxation acceleration, we show the trace distance between the time-evolved state $\varrho(t)$ and the steady state $\varrho_{\rm SS}$ as a function of the dimensionless time γt for different initial temperatures T in Fig. 3(c). We present four specific temperatures: $T = 7$ (dark blue dotted line), $T = 9$ (blue dashdotted line), $T = 11.13$ (red solid line), and $T = 18$ (dark red dashed line). During the initial dynamics, the trace distance decreases exponentially as $D(\varrho(t), \varrho_{\rm SS}) \sim \exp({\rm Re}(\lambda_4)t)$, independent of the initial distance between the thermal states (at different temperatures) and the steady state. Then, when the time approaches $\gamma t \approx 2.5$, the behaviors diverge. The time-evolved trace distance for the case of $T = 11.13$ maintains the highest relaxation rate, while for the other three temperature cases, the long-time dynamics cross over to a slower relaxation regime $\propto \exp({\rm Re}(\lambda_2)t)$ [see the Supplemental Material (SM) [59] for details]. Figure 3(c) therefore demonstrates the Mpemba effect: the hotter state at $T = 11.13$ exhibits an exceptional speedup and reaches the steady state faster than the colder states at $T = 7$ and $T = 9$. We further confirm that all four relaxation trajectories are overall cooling processes through their energy dynamics [see SM [59] for details]; together, these results establish the canonical quantum Mpemba effect.

We further quantify the acceleration capability of the canonical quantum Mpemba effect by defining the effective velocity $v_{\rm eff}$, which is the ratio of the initial trace distance to the critical time, $v_{\rm eff} = D(\varrho_{\rm th}[T], \varrho_{\rm SS})/(t_{\rm c}[T])$. The solid line in Fig. 3(d) shows $v_{\rm eff}$ as a function of T. We find that $v_{\rm eff}$ decreases with increasing temperature, and reaches a minimum around the steady-state effective temperature $T_{\rm SS} \approx 5.77$. This can be understood because the initial trace distance is minimized at this temperature, while the critical time is still finite, i.e., $D(\varrho_{\rm th}[T], \varrho_{\rm SS}) \to 0$ and $t_{\rm c}[T] \to {\rm const.}$, leading to the slowest effective velocity. After that, the effective velocity $v_{\rm eff}$ increases and exhibits a sharp peak around $T \approx 11.13$. Within this regime, the relaxation acceleration increases monotonically as a function of temperature. We refer to this as the Mpemba zone, highlighted by the gray-shaded area in Fig. 3(d).

Liouvillian Exceptional Point

In the present dissipative-qubit model, the temperature-controlled cancellation of the slowest Liouvillian mode is linked to the presence of a LEP [31,32,51]. In this work, the non-zero eigenvalues of $\mathcal{L}$ are analytically expressed as:

$$\lambda_k = -2\gamma + 2\sqrt{\frac{-R}{3}}\cos\left(\frac{1}{3}\arccos\left(-\frac{3Q}{2|R|}\sqrt{\frac{-3}{R}}\right) - \frac{2\pi k}{3}\right), \tag{6}$$

where $Q = -6\gamma\omega_y^2 + 4\gamma\omega_z^2 - 3\gamma^3/4$, $R = 4(\omega_y^2 + \omega_z^2) - 7\gamma^2/4$, and $k = 2, 3, 4$ [see SM [59] for details]. Figures 4(a) and 4(b) show the real and imaginary parts of the eigenvalues λ_k as a function of the dissipation γ, respectively. We observe that the LEP occurs near $\gamma \approx 4$. For clarity, the branches are labeled by continuous tracking from $\gamma > \gamma_{\rm EP}$, where ${\rm Re}(\lambda_2) > {\rm Re}(\lambda_3) > {\rm Re}(\lambda_4)$; at the LEP, the λ_2 and λ_3 branches coalesce, while below it they form a complex-conjugate pair. Before reaching the LEP, $\lambda_2 = \lambda_3^*$, preventing the elimination of c_k $(k = 2, 3)$ for thermal initial states [51,59]. Only when λ_2 is real does a critical temperature exist that satisfies $c_2 = 0$, e.g., $\gamma = 5$. We locate the eigenvalue degeneracy via the discriminant $\Delta = (Q/2)^2 + (R/3)^3$, where $\Delta > 0$ yields one real and two complex-conjugate eigenvalues, while $\Delta \le 0$ gives three real eigenvalues. The condition $\Delta = 0$ identifies the coalescing eigenvalues, while the geometric-multiplicity analysis provided in the SM confirms that this degeneracy is defective and hence

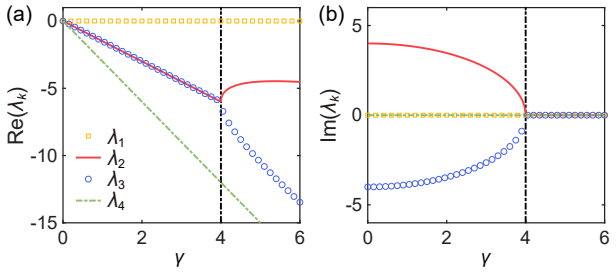

Fig. 4. The spectrum of Liouvillian $\mathcal{L}$. (a) The real part and (b) the imaginary part of the eigenvalues λ_k as a function of the decay strength γ. The yellow squares, red solid, blue circles and green dashed line denote the eigenvalues λ_1, λ_2, λ_3, and λ_4, respectively. The other parameters are $\omega_y = 0.01$ and $\omega_z = 2$.

constitutes a second-order LEP [59]. In this work, the canonical quantum Mpemba effect is discussed away from the LEP, where the Liouvillian is diagonalizable.

Experimental Feasibility

Equation (1) can be readily implemented using currently available quantum simulation technologies combined with quantum collision models. Quantum collision models have been widely used in simulations of open quantum systems [63–68], and have been experimentally realized [69–73]. This approach provides a discrete-time framework for open quantum dynamics: the environment is simulated as a collection of ancillas, denoted by η_{A}^n, $(n = 1, 2, \ldots)$. The system's continuous interaction with its environment is discretized into a sequence of pairwise unitary interactions ("collisions") between the system and individual ancillas, after which the ancillas are discarded. The system's stroboscopic evolution is thus generated by composing these elementary collision steps. Specifically, the system's reduced density matrix after the $(n+1)$-th collision is obtained through the map: $\varrho_{\mathrm{S}}^n \mapsto \varrho_{\mathrm{S}}^{n+1} = \mathrm{tr}_{\eta_{\mathrm{A}}^{n+1}}[U_{\mathrm{I}} U_{\mathrm{S}} \varrho_{\mathrm{S}}^n \otimes \eta_{\mathrm{A}}^{n+1} U_{\mathrm{S}}^\dagger U_{\mathrm{I}}^\dagger]$, where $U_{\mathrm{S}} = \exp(-\mathrm{i} H_{\mathrm{S}} \tau)$ governs the free evolution, $U_{\mathrm{I}} = \exp(-\mathrm{i} g H_{\mathrm{I}} \tau)$ describes the interactions, τ denotes the collision duration, and g is the interaction strength. We simulate the two baths using two sets of ancillas, $\{A_1\}$ and $\{A_2\}$, as illustrated in Fig. 5. The interaction Hamiltonian is $H_{\mathrm{I}} = H_{\mathrm{I}}^1 + H_{\mathrm{I}}^2 = (\sigma_{\mathrm{S}}^x \sigma_{A,1}^x + \sigma_{\mathrm{S}}^y \sigma_{A,1}^y)/2 + \sigma_{\mathrm{S}}^y \sigma_{A,2}^x$, with all ancillas initialized in the $|0\rangle$ state, i.e., a zero-temperature state. In the continuous-time limit ($\tau \to 0$), we recover the master equation [Eq. (1)], where $\gamma = g^2 \tau$ (see SM [59] for details). Each collision-step unitary is then mapped onto a quantum circuit by decomposing it into qubit rotations, Hadamard, and CNOT gates,

$$
\begin{aligned}
U_{\mathrm{S}} &= R_{\mathrm{S}}^x(\alpha) R_{\mathrm{S}}^z(2\Omega\tau) R_{\mathrm{S}}^x(-\alpha), \\
U_{\mathrm{I}}^1 &= R_{\mathrm{S}}^z\left(\frac{\pi}{2}\right) H_{A_1} \mathrm{CNOT}_{A_1,\mathrm{S}} R_{\mathrm{S}}^y(\theta) R_{A_1}^y(\theta) \mathrm{CNOT}_{A_1,\mathrm{S}} R_{\mathrm{S}}^z\left(-\frac{\pi}{2}\right) H_{A_1}, \\
U_{\mathrm{I}}^2 &= R_{\mathrm{S}}^x\left(\frac{\pi}{2}\right) H_{A_2} \mathrm{CNOT}_{A_2,\mathrm{S}} R_{A_2}^z(2\theta) \mathrm{CNOT}_{A_2,\mathrm{S}} R_{\mathrm{S}}^x\left(-\frac{\pi}{2}\right) H_{A_2},
\end{aligned}
\tag{7}
$$

where $\Omega = \sqrt{\omega_y^2 + \omega_z^2}$, $\alpha = \arctan 2(\omega_y, \omega_z)$, and $\theta = g\tau$. The partial-trace operation is implemented by resetting the ancillas after each collision, which allows them to be reused in subsequent steps and reduces the required hardware to a simple $A_1 - S - A_2$ chain [see Fig. 1(c)]. Since thermal (Gibbs) state initialization in a quantum circuit is generally nontrivial [74], we bypass direct initialization and exploit the linearity of the master equation in ϱ_{th}, writing its evolution as $\varrho_{\mathrm{th}}(t) = \sum_j P_j \exp(t\mathcal{L})[\varrho_j]$, where $\varrho_{\mathrm{th}} = \sum_j P_j |\psi_j\rangle\langle\psi_j| = \sum_j P_j \varrho_j$, and P_j is the probability of the pure state $|\psi_j\rangle$. By incorporating classical processing, one can reconstruct the evolution of a given thermal state [see Fig. 1(c)]. We verify the feasibility of our hybrid classical-quantum algorithm on the state-of-the-art quantum device. Detailed discussion and experimental results can be found in SM [59].

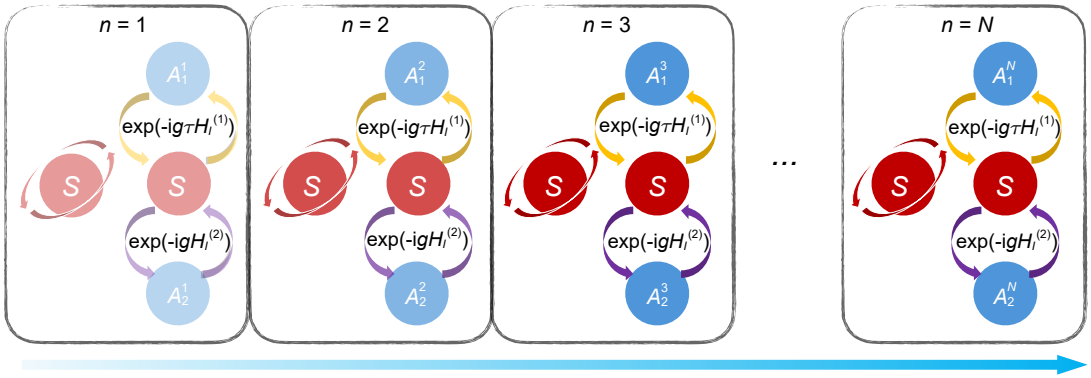

Fig. 5. Schematic of the quantum collision model to realize Eq. (1). The system qubit S interacts sequentially with two types of ancillas, A_1 and A_2, which are prepared in $|0\rangle$ state. Each interaction is followed by a partial trace over the ancillas, simulating the effect of the environment.

Conclusions

In summary, we have introduced the canonical quantum Mpemba effect and demonstrated its occurrence in a dissipative qubit system. By defining the steady-state effective temperature and examining the energy dynamics, we showed that each relaxation evolves from a higher-temperature, higher-energy thermal state toward a steady state with a lower effective temperature and energy, and can therefore be characterized as an overall cooling process. Notably, within the Mpemba zone, the relaxation dynamics exhibit exponential acceleration as the initial temperature increases. This work provides the quantum analogue of the classical Mpemba effect, highlighting the fundamental role of temperature in anomalous relaxation dynamics, and offers a practical collision-model scheme for simulating the corresponding dissipative evolution using superconducting qubits. We anticipate that our findings can be extended to open quantum many-body systems, and thereby spur further studies of anomalous non-equilibrium phenomena.

Data Availability

The data that support the findings of this study are openly available [75].

Acknowledgments

The authors thank Jiasen Jin, Wenlin Li, and Jinghui Pi for reviewing the manuscript. This work was supported by the Quantum Science and Technology-National Science and Technology Major Project (Grant No. 2024ZD0300600), the China Manned Space Program (Grant No. KJZ-YY-NWL-0502), the National Natural Science Foundation of China (Grant No. 92565105), the Hong Kong RGC (Grant Nos. 14301425, 24308323, and C4050-23GF), the Guangdong

Strategic Initiative for Quantum Science (Grant Nos. GDZX2505005 and GDZX2404004), and the CUHK Direct Grant.

References

[1] Mpemba E B and Osborne D G 1969 *Phys. Educ.* **4** 172
[2] Ares F, Calabrese P, and Murciano S 2025 *Nat Rev Phys* **7** 451
[3] Lapolla A and Godec A 2020 *Phys. Rev. Lett.* **125** 110602
[4] Yamashika S, Calabrese P, and Ares F 2025 *Phys. Rev. A* **111** 043304
[5] Klobas K, Rylands C, and Bertini B 2025 *Phys. Rev. B* **111** L140304
[6] Alyürük D C, Yeşiller M H, Vedral V, and Pusuluk O 2025 arXiv: 2502.00123 [quant-ph]
[7] Summer A, Moroder M, Bettmann L P, Turkeshi X, Marvian I, and Goold J 2026 *Phys. Rev. X* **16** 011065
[8] Van Vu T and Hayakawa H 2025 *Phys. Rev. Lett.* **134** 107101
[9] Teza G, Bechhoefer J, Lasanta A, Raz O, and Vucelja M 2026 *Phys. Rep.* **1164** 1
[10] Turkeshi X, Calabrese P, and De Luca A 2025 *Phys. Rev. Lett.* **135** 040403
[11] Ares F, Murciano S, and Calabrese P 2023 *Nat. Commun.* **14** 2036
[12] Liu S, Zhang H K, Yin S, and Zhang S X 2024 *Phys. Rev. Lett.* **133** 140405
[13] Rylands C, Klobas K, Ares F, Calabrese P, Murciano S, and Bertini B 2024 *Phys. Rev. Lett.* **133** 010401
[14] Yamashika S, Ares F, and Calabrese P 2024 *Phys. Rev. B* **110** 085126
[15] Yu H, Hu J, and Zhang S X 2026 *Phys. Rev. B* **113** 134304
[16] Yamashika S and Ares F 2026 *Phys. Rev. Lett.* **136** 090402
[17] Bhore T, Su L, Martin I, Clerk A A, and Papić Z 2025 *Phys. Rev. B* **112** L121109
[18] Ares F, Rylands C, and Calabrese P 2025 *J. Phys. A: Math. Theor.* **58** 445302
[19] Chang W X, Yin S, Zhang S X, and Li Z X 2026 *Phys. Rev. Lett.* **136** 100403
[20] Gibbins M, Smith A, and Bertini B 2025 *Phys. Rev. B* **112** L180307
[21] Liu S, Zhang H K, Yin S, Zhang S X, and Yao H 2025 *Sci. Bull.* **70** 3991
[22] Sugimoto K, Kuwahara T, and Saito K 2025 arXiv: 2507.04669 [cond-mat.stat-mech]
[23] Yu Y H, Jin T R, Zhang L, Xu K, and Fan H 2025 *Phys. Rev. B* **112** 094315
[24] Carollo F, Lasanta A, and Lesanovsky I 2021 *Phys. Rev. Lett.* **127** 060401
[25] Nava A and Egger R 2024 *Phys. Rev. Lett.* **133** 136302
[26] Chatterjee A K, Takada S, and Hayakawa H 2023 *Phys. Rev. Lett.* **131** 080402
[27] Strachan D J, Purkayastha A, and Clark S R 2025 *Phys. Rev. Lett.* **134** 220403
[28] Medina I, Culhane O, Binder F C, Landi G T, and Goold J 2025 *Phys. Rev. Lett.* **134** 220402
[29] Tejero Á, Sánchez R, Kaoutit L E, Manzano D, and Lasanta A 2025 *Phys. Rev. Res.* **7** 023020
[30] Wang X and Wang J 2024 *Phys. Rev. Res.* **6** 033330
[31] Zhou Y L, Yu X D, Wu C W, Li X Q, Zhang J, Li W, and Chen P X 2023 *Phys. Rev. Res.* **5** 043036
[32] Chatterjee A K, Takada S, and Hayakawa H 2024 *Phys. Rev. A* **110** 022213
[33] Moroder M, Culhane O, Zawadzki K, and Goold J 2024 *Phys. Rev. Lett.* **133** 140404
[34] Longhi S 2024 *Opt. Lett.* **49** 5188
[35] Longhi S 2024 *APL Quantum* **1** 046110
[36] Dong J W, Mu H F, Qin M, and Cui H T 2025 *Phys. Rev. A* **111** 022215
[37] Caceffo F, Murciano S, and Alba V 2024 *J. Stat. Mech.* **2024** 063103
[38] Boubakour M, Endo S, Fogarty T, and Busch T 2025 *Quantum Sci. Technol.* **10** 025036
[39] Liu D, Yuan J, Ruan H, Xu Y, Luo S, He J, He X, Ma Y, and Wang J 2024 *Phys. Rev. A* **110** 042218
[40] Su Y, Qi F, and Jin G 2025 *Phys. Rev. B* **111** 125404
[41] Zhao M and Hou Z 2026 *Commun. Phys.* **9** 192
[42] Longhi S 2025 *APL Quantum* **2** 026133
[43] Ma W and Liu J 2025 *Phys. Rev. B* **112** 214310
[44] Nava A and Egger R 2025 *Phys. Rev. Lett.* **135** 140404
[45] Qian D, Wang H, and Wang J 2025 *Phys. Rev. B* **111** L220304
[46] Graf J, Splettstoesser J, and Monsel J 2025 *J. Phys.: Condens. Matter* **37** 195302
[47] Ramon-Escandell C, Prositto A, and Segal D 2025 *Phys. Rev. Res.* **7** 043012
[48] Wang Z M, Wu S L, Byrd M S, and Wu L A 2024 arXiv: 2411.17197 [quant-ph]
[49] Bao R and Hou Z 2025 *Phys. Rev. Lett.* **135** 150403
[50] Wei Z, Xu M, Jiang X P, Hu H, and Pan L 2026 *Sci. China Phys. Mech. Astron.* **69** 240315
[51] Zhang J, Xia G, Wu C W, Chen T, Zhang Q, Xie Y, Su W B, Wu W, Qiu C W, Chen P X, Li W, Jing H, and Zhou Y L 2025 *Nat. Commun.* **16** 301
[52] Aharony Shapira S, Shapira Y, Markov J, Teza G, Akerman N, Raz O, and Ozeri R 2024 *Phys. Rev. Lett.* **133** 010403
[53] Joshi L K, Franke J, Rath A, Ares F, Murciano S, Kranzl F, Blatt R, Zoller P, Vermersch B, Calabrese P, Roos C F, and Joshi M K 2024 *Phys. Rev. Lett.* **133** 010402
[54] Xu Y, Fang C P, Chen B J *et al.* 2026 *Phys. Rev. Lett.* **137** 010402
[55] Breuer H P and Petruccione F 2010 *The Theory of Open Quantum Systems* (Oxford: Oxford University Press)
[56] Trushechkin A S, Merkli M, Cresser J D, and Anders J 2022 *AVS Quantum Sci.* **4** 012301
[57] Sun S K and Chen S 2024 *Phys. Rev. B* **110** 134301
[58] Nielsen M A and Chuang I L 2010 *Quantum Computation and Quantum Information 10th Anniversary Edition* (New York: Cambridge University Press)
[59] See Supplemental Material for the analytic Liouvillian solution, including the Liouvillian exceptional point and its Jordan-block structure; the energy and effective-temperature dynamics and heat currents; the derivation of the quantum master equation within the quantum collision-model framework; details of the quantum-circuit construction and experimental validation of the collision-model simulation of open-system evolution from a thermal initial state; and additional Refs. [60–62].
[60] Minganti F, Biella A, Bartolo N, and Ciuti C 2018 *Phys. Rev. A* **98** 042118
[61] Ciccarello F, Lorenzo S, Giovannetti V, and Palma G M 2022 *Phys. Rep.* **954** 1
[62] Lacroix T, Cilluffo D, Huelga S F, and Plenio M B 2025 *Commun. Phys.* **8** 268
[63] Cattaneo M, De Chiara G, Maniscalco S, Zambrini R, and Giorgi G L 2021 *Phys. Rev. Lett.* **126** 130403
[64] Landi G T 2022 *PRX Quantum* **3** 010303
[65] Erbanni R, Xu X, Demarie T F, and Poletti D 2023 *Phys. Rev. A* **108** 032619
[66] Zhang Q, Man Z X, Zhang Y J, Yan W B, and Xia Y J 2023 *Phys. Rev. A* **107** 042202
[67] Alves G O, Santos M A F, and Landi G T 2024 *Phys. Rev. A* **110** 052421
[68] Mahlow F, Çakmak B, Karpat G, Yalçınkaya İ, and Fanchini F F 2024 *Phys. Rev. A* **109** 052411
[69] Cuevas Á, Geraldi A, Liorni C, Bonavena L D, De Pasquale A, Sciarrino F, Giovannetti V, and Mataloni P 2019 *Sci. Rep.* **9** 3205
[70] García-Pérez G, Rossi M A C, and Maniscalco S 2020 *npj Quantum Inf.* **6** 1
[71] Cattaneo M, Rossi M A, García-Pérez G, Zambrini R, and Maniscalco S 2023 *PRX Quantum* **4** 010324
[72] Cech M, Lesanovsky I, and Carollo F 2023 *Phys. Rev. Lett.* **131** 120401
[73] Li X, Li Y, and Yan Y 2026 *Chin. Phys. Lett.* **43** 020302
[74] Consiglio M, Settino J, Giordano A, Mastroianni C, Plastina F, Lorenzo S, Maniscalco S, Goold J, and Apollaro T J G 2024 *Phys. Rev. A* **110** 012445
[75] Li X, Li Y, and Yan Y 2025 *Replication Data for: Canonical Quantum Mpemba Effect in a Dissipative Qubit*. [Dataset] https://doi.org/10.48668/MQUWVU